Stability of the RWM and its Stabilization by Plasma Rotation

Ming. S. Chu
General Atomics, San Diego, California 92186-5608

July 22, 2002

1 summary

Three numerical equilibria, two based on the proposed ITER-AT and one for the proposed FIRE-AT, have been tested for their stability to the RWM and stabilization of the RWM by plasma rotation. The MARS stability code is used in the study. For one of the ITER-AT equilibrium (ITER-AT-S, based on scenario 4, generated by Bulmer-Leuer-Lao and agreed to by Gribov), it is found that with a rigid rotor plasma rotation profile, a rotation frequency 1% of the Alfven frequency is sufficient to stabilize the RWM. Whereas with a given experimental rotation profile, the central plasma rotation required for RWM stabilization is around 5% of the Alfven rotation frequency. For the other ITER-AT equilibrium (ITER-AT-DN, based on an equilibrium generated by the MHD group at GA), the rotation required for a rigid rotor rotation profile is around 0.5% and the central plasma rotation required for the given experimental rotation profile is around 1% of the Alfven frequency. For the FIRE-AT (generated by Kessel), the rotation required for a rigid rotor rotation profile is around 1.5% and the central plasma rotation required for the given experimental rotation profile is around 6% of the Alfven frequency. A brief discussion of the effect of plasma dissipation and transport on these results is also included.

2 Analysis Procedure and the MARS Code

To analyze a given equilibrium for its stability to the RWM and to quantify the critical rotation speed which is needed for the stabilization, the linear eigenvalue code - MARS [1] is utilized.

2.1 MARS

MARS solves the linear MHD perturbation equations with the complex frequency (both the growth rate and the frequency) of the MHD mode as its eigenvalue. The eigenfunction is the complex perturbation of the basic MHD state variables. These are the plasma velocity, magnetic field, current components and pressure, in total ten two-dimensional variables. This code was extended to study the effect of a sheared plasma rotation profile on the stability of MHD modes [2].

2.2 Rotation Profile

For the stability of the RWM, one of the most important input quantities is the plasma rotation profile. At present, there is no comprehensive theory for the self-consistent determination of the plasma rotation profile. In general, the plasma angular momentum transport has been found to be anomalous and with an anomalous confinement time similar to the energy confinement time. Yet, the details of the energy transport and angular momentum transport are quite different. Because of this, we do not expect that a credible rotation profile can be predicted for the future devices such as ITER-AT or FIRE-AT. Nevertheless, a quantitative comparison of the performance of devices can be made, if the rotation profile is assumed to be the same. In this study, we assume two different possible profiles.

- An empirically determined profile. This is the experimentally observed rotation profile of the discharges in DIII-D RWM experiments, i.e., shot 106029 at 1500 $msec$. This rotation profile is shown in Fig. 1. In this figure, the ratio of the angular frequency (ω) to the central Alfven angular frequency

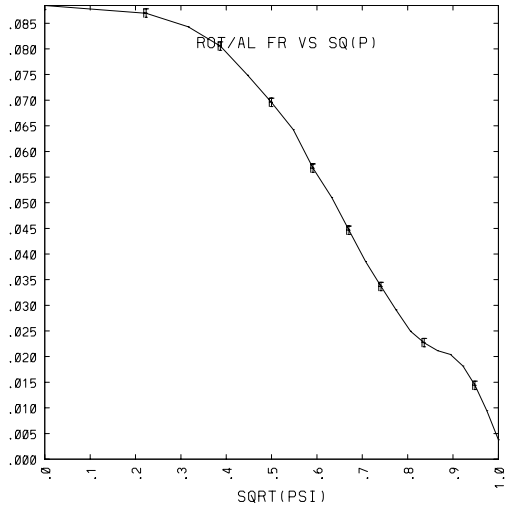

Figure 1: The rotation profile of shot 106029 at 1500ms of the DIII-D RWM experiment. The normalized rotation frequency ω/ω_{av} is plotted as a function of the square root of the poloidal flux function $\sqrt{\psi}$.

(ω_{av}) is plotted as a function of $\sqrt{\psi}$. Note that the Alfven angular rotation frequency is defined as

$$\omega_{av} = \frac{v_A}{R_{mid}} \tag{1}$$

and R_{mid} is the plasma center, defined as the average of the minimum and maximum radial locations on the boundary. The Alfven speed v_A is

$$v_A = \frac{B_{vac}}{\sqrt{\mu_0 \rho_0}} \tag{2}$$

and B_{vac} is the magnitude of the toroidal vacuum field at the location of R_{mid}

- **The rigid rotor profile. We assume that the plasma rotates as a rigid rotor. This is also a useful assumption if we can manage to imitate the rotation of the external wall when the plasma has negligible rotation speed.**

2.3 Damping of the Electromagnetic Angular Momentum by the Plasma

It has been pointed out that coupling of plasma dissipation with rotation of the plasma relative to an external resistive wall can lead to the stabilization of the RWM [3]. This stabilization effect has since been demonstrated experimentally [4]. However, the effectiveness of this stabilization mechanism depends not only on the plasma rotation profile, but also on the plasma mechanism that damps the electromagnetic perturbation. At the moment, there does not exist a comprehensive, experimentally verified, theory for this mechanism. However, there has been an empirical model which includes a variable coefficient. This model has been used to interpret experimental data. The variable coefficient has in turn been empirically determined by this process. This is the sound wave damping model. In this model, the force that damps the perturbed toroidal motion of the plasma is given by

$$F_{SD} = -\kappa_{\|}\sqrt{\pi}|k_{\|}v_{th_i}|\rho\vec{v}\cdot\hat{b}\hat{b}. \tag{3}$$

Here, $\kappa_{\|}$ is a numerical coefficient. The force given in Eq. (3) is intended to model the ion Landau damping process. In this formula, $k_{\|}$ is the parallel wave number $(m-nq)/R$, v_{th_i} is the ion thermal speed, ρ is the mass density, $\vec{v}$ is the perturbed plasma velocity and $\hat{b}$ is the unit vector of the equilibrium magnetic field. The value of $\kappa_{\|} = 0.89$ was tested in a previous analysis of experimental results in DIII-D [5] and shown to best fit the experimental data.

3 ITER-AT-S

3.1 Equilibrium

A numerical equilibrium (iter.Ped.AT.129 gfile) for the proposed ITER-AT scenario 4 was generated by Bulmer-Leuer-Lao and agreed to by Gribov. This is the input equilibrium. To generate the mapping quantities needed by MARS, a new up-down symmetric equilibrium is reconstructed by using TOQ with information from the input equilibrium. The reconstruction process uses the upper

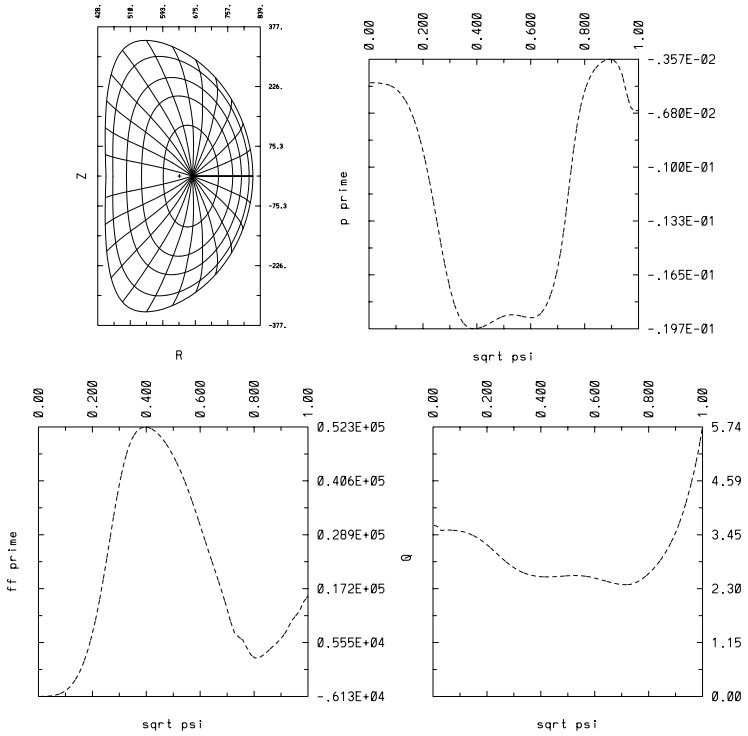

Figure 2: The reconstructed ITER-AT-S equilibrium. The poloidal flux function ψ in the poloidal $R-Z$ plane is plotted in the upper left corner. The pressure gradient p', the current density ff' and the safety factor q are plotted as functions of $\sqrt{\psi}$ in the upper right, lower left and lower right, respectively.

plasma boundary and pressure gradient and current profiles from the input equilibrium. The reconstructed equilbrium has $R_0 = 635$ cm**,** $r_p = 185$ cm**,** $I_p = 9$ MA**,** $\beta_n = 2.64$**,** $q_{min} = 2.38$**,** $q_{95} = 4.95$ **and** $\beta =< p > /B_0^2 = 2.474\%$**. Here,** $B_0 = 5.175$ T **at** R_0**. The** $2-D$ **flux plot as a function of** R **and** Z**, together with the pressure gradient** p'**, the current gradient** ff' **and the safety factor** q **profiles as a function of** $\sqrt{\psi}$ **are shown in Fig. 2. It is interesting to note that this equilibrium has no** $q = 2$ **surface. All the singular surfaces for** $n = 1$ **perturbations** $(q = 3, 4, 5)$ **are concentrated at the plasma edge.**

3.2 Stability Results

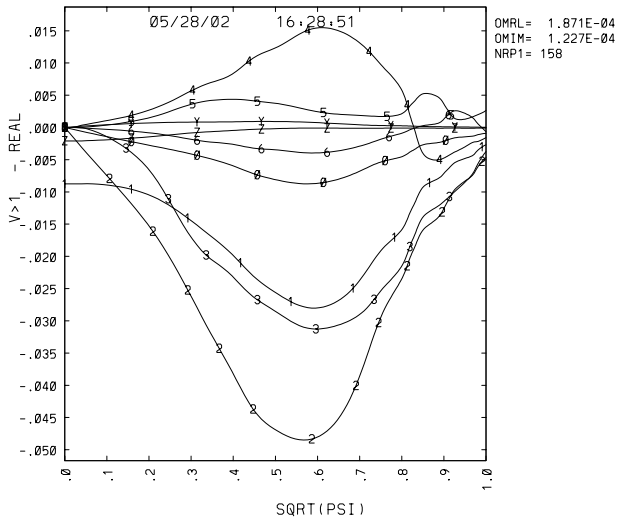

Figure 3: Various Fourier components of the perturbed velocity of an unstable RWM in the ITER-AT-S equilibrium as a function of $\sqrt{\psi}$. Here, ψ is the equilibrium poloidal flux function.

In the MARS analysis, the grid size used was 158 plasma surfaces and 40 surfaces in the vacuum region. The external computing boundary is located at $r_{boundary}/r_{plasma} = 2.0$ and 20 Fourier harmonics are used. The TOQ equilibrium was first tested by DCON for its stability to the external kink mode. DCON found that the marginal stability location of the external wall is at $r_{idealwall}/r_{plasma} =$ 1.44. Shown in Fig. 3 is the a typical eigenfunction produced by MARS. It gives the mode amplitude of the various poloidal Fourier harmonics of the radial velocity perturbations of an unstable resistive wall mode in this equilibrium as a function of $\sqrt{\psi}$, with ψ being the equilibrium poloidal flux function. It is observed that this mode has a global structure. It is interesting to note that as the plasma gets less stable to the resistive wall mode, its edge perturbation becomes larger relative to the inside.

Shown in Fig. 4 is the growth rate of the resistive wall mode as

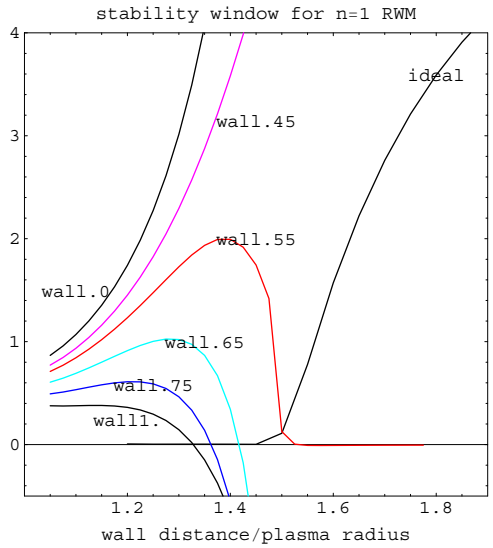

Figure 4: Stability window of the RWM versus wall location for the ITER-AT-S equilibrium. The rotation profile from DIII-D experiment Shot 106029 at 1500 $msec$ is used. Plotted are growth rates multiplied by τ_w of the ideal and resistive wall modes versus r_w. The curve labeled ideal is the growth rate of the ideal external kink divided by 25. Other curves are labeled by the fraction of the input DIII-D rotation frequency used.

a function of the location of the resistive wall. Each curve has a different plasma central rotation frequency relative to the resistive wall. The same equilibrium is used here as in Fig. 3.

Fig. 4 shows that the marginal location of the ideal wall predicted by MARS for the ideal external kink is at ~ 1.49. This is in close agreement with that given by DCON. In conjunction with Fig. 1, we can see that the critical central rotation freqency for stabilization of the RWM is $\omega_{central}/\omega_{av} = 0.05$. We have noted before, that the ITER-AT-S equilibrium does not have a $q = 2$ resonant surface. The $q = 3, 4, 5$ resonances are located at the plasma edge where the rotation frequencies are much lower than the center. To understand the results in Fig. 4 better, we also performed the stability analysis for the rigid rotor plasma rotation profile. This is a viable scenario because recently there has appeared a proposal on

the possible utilization of a rotating (flowing) liquid wall. Shown in Fig. 5 is the results for rigid plasma rotation. Comparing this

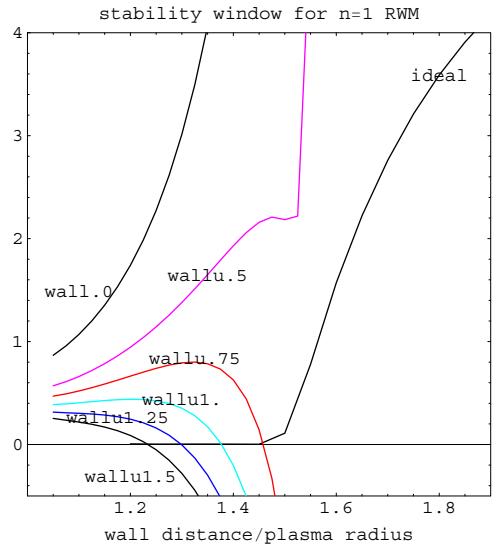

Figure 5: Stability window of the RWM versus wall location for the ITER-AT-S with a rigid plasma rotation profile. Plotted are growth rates multiplied by τ_w of the ideal and resistive wall modes versus r_w. The curve labeled ideal is the growth rate of the ideal external kink divided by 25. Other curves are labeled by the rotation frequency of the rigid plasma rotation measured in units of percent of the toroidal Alfven transit frequency.

figure with that from nonuniform rotation, we note that the required rotations at the plasma center differ by a factor of 5. This indicates that the rotation requirement for stabilization is more closely related to the rotation speed at the lower order rational surfaces ($q = 3, 4, 5$).

4 ITER-AT-DN

To study the effect of equilibrium variation on the required plasma rotation for the stabilization of the RWM, an additional ITER equilibrium based on a doulbe null configuration is examined.

4.1 Equilibrium

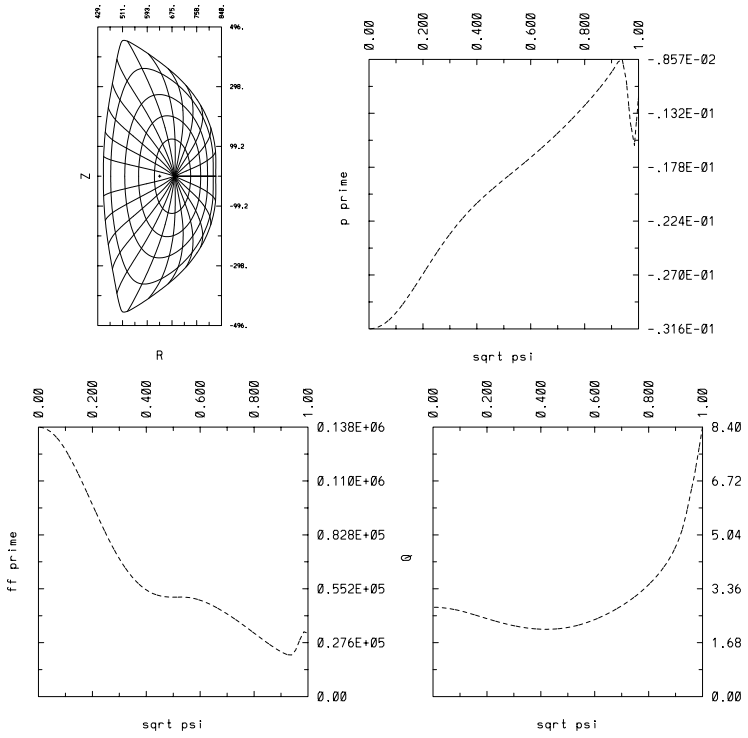

Figure 6: The reconstructed ITER-AT-DN equilibrium. The poloidal flux function ψ in the poloidal $R - Z$ plane is plotted in the upper left corner. The pressure gradient p', the current density ff' and the safety factor q are plotted as functions of $\sqrt{\psi}$ in the upper right, lower left and lower right, respectively.

The input numerical equilibrium is the iter.wrs.d3d.4.129 gfile, an equilibrium with a lower single null. This is an equilibrium porposed by the GA team for the advanced ITER operation. The equilibrium reconstruction utilized the pressure gradient and current profiles from this input equilibrium and the lower half of the plasma boundary. The upper boundary is obtained from reflection to obtain an up-down symmetric plasma boundary. The β value is adjusted with fixed $< j.B >$ profile so that the location for marginal stability with respect to the ideal external kink mode is at

$r_w/plasmaradius = 1.5$. **One consequence of this modification of the equilibrium is that the q profile has its minimum slightly above 2 and the q value increases relatively quickly to a large value near the plasma edge, but at the same time covers a relatively large portion of the plasma volume during this increase in q. The reconstructed equilbrium has $R_0 = 634\ cm$, $r_p = 187\ cm$, $I_p = 10.1\ MA$, $\beta_n = 3.22$, $q_{min} = 2.1$, $q_{95} = 7.11$ and $\beta =< p > /B_0^2 = 3.3\%$. In here, $B_0 = 5.3\ T$ at R_0. The $2-D$ flux plot as a function of R and Z, together with the pressure gradient p', the current gradient ff' and the safety factor q profiles as a function of $\sqrt{\psi}$ are shown in Fig. 6 We note that this equilibrium has q_{min} close to 2.**

4.2 Stability Results

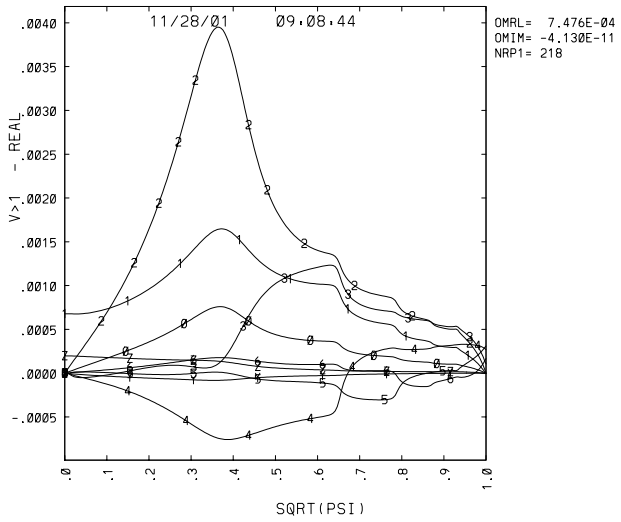

Figure 7: Various Fourier components of the perturbed velocity of an unstable RWM in the ITER-AT-DN equilibrium as a function of $\sqrt{\psi}$. Here, ψ is the equilibrium poloidal flux function.

The TOQ equilibrium was first tested by DCON for its stability to the external kink mode. DCON found that the marginal stability location of the external wall is at $r_{idealwall}/r_{plasma} = 1.5$. Shown in

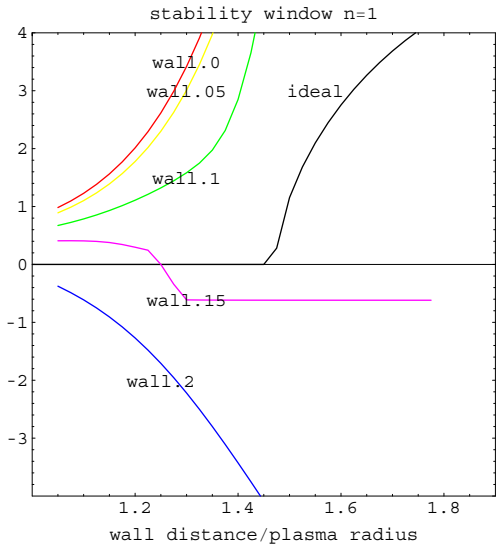

Figure 8: Stability window of the RWM versus wall location for the ITER-AT-DN equilibrium. The rotation profile from DIII-D experiment Shot 106029 at 1500 $msec$ is used. Plotted are growth rates multiplied by τ_w of the ideal and resistive wall modes versus r_w. The curve labeled ideal is the growth rate of the ideal external kink divided by 25. Other curves are labeled by the fraction of the input DIII-D rotation frequency used.

Fig. 7 is the a typical eigenfunction produced by MARS. It gives the mode amplitude of the various poloidal Fourier harmonics of the radial velocity perturbations of an unstable resistive wall mode in this equilibrium as a function of $\sqrt{\psi}$, with ψ being the equilibrium poloidal flux function. It is observed that this mode has a pronounced $m = 2$ component.

Shown in Fig. 8 is the growth rate of the resistive wall mode as a function of the location of the resistive wall. Each curve has a different plasma central rotation frequency relative to the resistive wall. The same equilibrium is used here as in Fig. 7.

Fig. 8 shows that the marginal location of the ideal wall predicted by MARS for the ideal external kink is at ~ 1.5. This is in close agreement with that given by DCON. In conjunction with Fig. 1, we can see that the critical central rotation freqency for

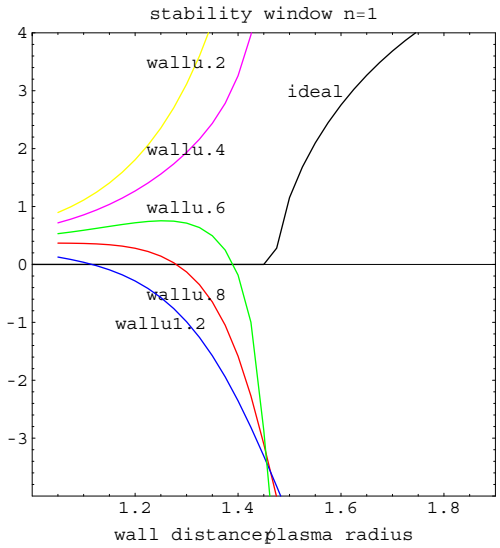

Figure 9: Stability window of the RWM versus wall location for the ITER-AT-DN with a rigid plasma rotation profile. Plotted are growth rates multiplied by τ_w of the ideal and resistive wall modes versus r_w. The curve labeled ideal is the growth rate of the ideal external kink divided by 25. Other curves are labeled by the rotation frequency of the rigid plasma rotation measured in units of percent of the toroidal Alfven transit frequency.

stabilization of the RWM is between $\omega_{central}/\omega_{av} = 0.008$ to 0.012. No stability window is found for rotation frequency below 0.008. The stability window for the location of the resistive wall is between 1.2 and 1.5 of the plasma radius when the central plasma rotation frequency is at 0.012 of the Alfven frequency. This window widens to between 1.0 to 1.5 of the plasma radius when the central rotation frequency is increased to 0.016 of the Alfven frequency. To understand the results in Fig. 8 better, we also performed the stability analysis for the rigid rotor plasma rotation profile. This is a viable scenario because recently there has appeared a proposal on the possible utilization of a rotating (flowing) liquid wall. Shown in Fig. 9 is the results for rigid plasma rotation. Comparing this figure with that from nonuniform rotation, we note that the required rotations at the plasma center differ by a factor of 2. This

indicates that the rotation requirement for stabilization is related to the structure of the eigenfunction, i.e. the eigenfunction is more peaked towards the central part of the plasma, where the damping is strong. Nevertheless, the rigid rotation model is still more effective than a profiled rotation, indicating that the sum of the effects at the higher q surfaces still carry a larger portion of the weight in providing the damping of the RWM (cf. Eq. (3)).

5 FIRE-AT

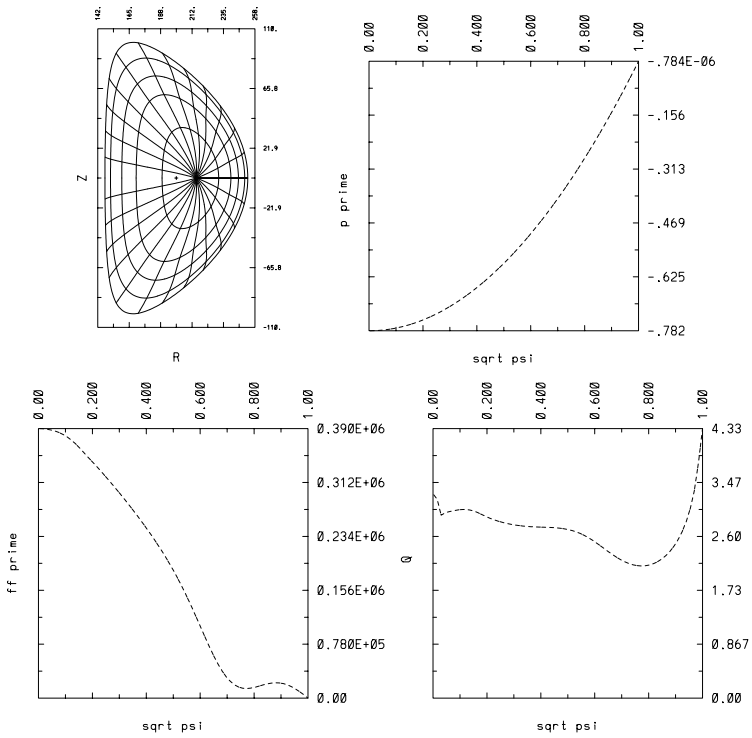

Figure 10: The reconstructed FIRE-AT equilibrium. The reconstructed poloidal flux function ψ in the poloidal $R - Z$ plane is plotted in the upper left corner. The pressure gradient p', the current density ff' and the safety factor q are plotted as functions of $\sqrt{\psi}$ in the upper right, lower left and lower right, respectively.

The input equilibrium, produced by using the JSOLVER code for the FIRE-AT, was obtained from Kessel. The new equilibrium reconstructed by using TOQ with the boundary and profile information from the input JSOLVER equilibrium has $R_0 = 200\ cm$, $r_p = 52.5\ cm$, $I_p = 5.4\ MA$, $\beta_n = 3.62$, $q_{min} = 2.13$, $q_{95} = 3.45$, and $\beta =< p > /B_0^2 = 4.38\%$. Here, $B_0 = 8.5\ T$ at R_0. The $2-D$ flux plot as a function of R and Z, together with the pressure gradient p', the current gradient ff' and the safety factor q profiles as a function of $\sqrt{\psi}$ are shown in Fig. 10.

We note that this equilibrium has no $q = 2$ surface. The two singular surfaces for the $n = 1$ perturbations ($q = 3, 4$) are located near the plasma edge.

5.1 Stability Results

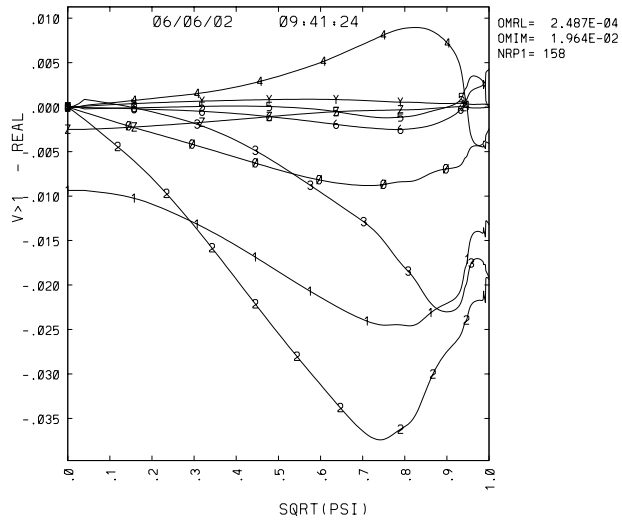

Figure 11: Various Fourier components of the perturbed velocity of an unstable RWM as a function of $\sqrt{\psi}$ for the FIRE-AT equilibrium. Here, ψ is the equilibrium poloidal flux function.

In the MARS analysis, the grid size used was 158 plasma surfaces and 40 surfaces in the vacuum region. The external comput-

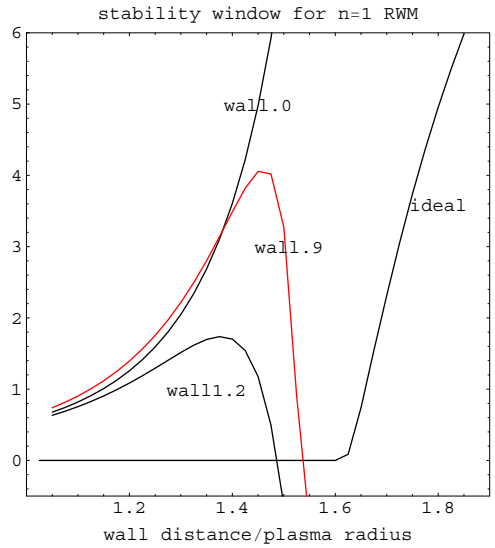

Figure 12: Stability window of the RWM versus wall location for the FIRE-AT equilibrium. The rotation profile from DIII-D experiment Shot 106029 at 1500 $msec$ is used. Plotted are growth rates multiplied by τ_w of the ideal and resistive wall modes versuss r_w. The curve labeled ideal is the growth rate of the ideal external kink divided by 25. Other curves are labeled by the fraction of the input DIII-D rotation frequency used.

ing boundary is located at $r_{boundary}/r_{plasma} = 2.0$ and 20 Fourier harmonics are used. The TOQ equilibrium was first tested by DCON for its stability to the external kink mode. DCON found that the marginal stability location of the external wall is at $r_{idealwall}/r_{plasma} =$ 1.65.

Shown in Fig. 11 is the a typical eigenfunction produced by MARS. It gives the mode amplitude of the various poloidal Fourier harmonics of the radial velocity perturbations of an unstable resistive wall mode in this equilibrium as a function of $\sqrt{\psi}$, with ψ being the equilibrium poloidal flux function. It is observed that this mode has a global structure. It is interesting to note that as the plasma gets less stable to the resistive wall mode, its edge perturbation becomes larger relative to the inside.

Shown in Fig. 12 is the growth rate of the resistive wall mode

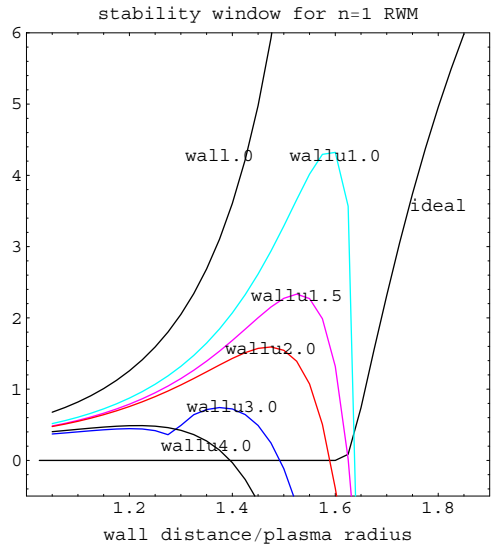

Figure 13: Stability window of the RWM versus wall location for the FIRE-AT for rotation with rigid plasma rotation profile. Plotted are growth rates multiplied by τ_w of the ideal and resistive wall modes versus r_w. The curve labeled ideal is the growth rate of the ideal external kink divided by 25. Other curves are labeled by the rotation frequency of the rigid plasma rotation measured in units of percent of the toroidal Alfven transit frequency.

as a function of the location of the resistive wall. Each curve has a different plasma central rotation frequency relative to the resistive wall. The same equilibrium is used here as in Fig. 11.

Fig. 12 shows that the marginal location of the ideal wall predicted by MARS for the ideal external kink is at ~ 1.65. This is in close agreement with that given by DCON. In conjunction with Fig. 1, we can see that the critical central rotation freqency for stabilization of the RWM is $\omega_{central}/\omega_{av} = 0.06$. We have noted before that the FIRE-AT equilibrium does not have a $q = 2$ resonant surface. The $q = 3, 4$ resonances are located at the plasma edge where the rotation frequencies are much lower than the center. To understand the results in Fig. 12 better, we also performed the stability analysis for the rigid rotor plasma rotation profile. This is a viable scenario because recently there has appeared a proposal on

the possible utilization of a rotating (flowing) liquid wall. Shown in Fig. 13 is the results for rigid plasma rotation. Comparing this figure with that from nonuniform rotation, we note that the required rotations at the plasma center differ by a factor of 4. This indicates that the rotation equirement for stabilization is related to the rotation speed at the lower order rational surfaces ($q = 3, 4$).

6 DISCUSSION

The effect of plasma rotation on the stability of the RWM has been studied by using the MARS code on the three equilibria ITER-AT-S, ITER-AT-DN and the FIRE-AT. Amongst these, the ITER-AT-DN configuration gives the least stringent requirement on the necessary plasma rotation, i.e. 0.5% of the Alfven frequency for rigid plasma rotation. The basis of this projection was that dissipation in the plasma will allow the plasma to transfer momentum to the electro-magnetic perturbation to stabilize the RWM[3]. The details of this momentum transfer mechanism is therefore extremely important. The mechanism used in the present study was based on the experimentally fitted formula based on Eq. (3). Although there is some theoretical basis for this model, it is important to have further theoretical and experimental effort aimed at fully clarifying the validity of this model. Another important input in the present study is the plasma rotation profile. At the moment, this quantity is not completely understood. It involves the input of the toroidal angular momentum by the source and the transport equilibration of the angular momentum by the plasma. A more comprehensive investigation of these topics is necessary before we can quantitatively understand the power requirement for driving the plasma rotation for the stabilization of the RWM.

7 ACKNOWLEDGMENTS

The author would like to achknowledge Dr. Vincent Chan, Chris Hegna and Ted Strait for suggestions on the contents of this report and Prof. Jim Callen for detailed comments on the write up.

References

[1] A. Bondeson, G. Vlad, and H. Lutjens, Phys. Fluids B4, 1889 (1992).

[2] M.S. Chu, R.L. Miller, A. Bondeson, H. Lutjens, G. DeRidder, and O. Sauter, Proceedings of 22nd EPS, Bournemouth, UK, Controlled Fusion and Plasma Physics, 19C, I-241 (1995).

[3] A. Bondeson and D. Ward Phys. Rev. Lett. 72, 2709 (1994).

[4] A.M. Garofalo, T.H. Jensen, L.C. Johnson, R.J. LaHaye, G.A. Navratil, M. Okabayashi, J.T. Scoville, E.J. Strait, D.R. Baker, J. Bialek, M.S. Chu, J.R. Ferron, J. Jayakumar, L.L. Lao, M.A. Makowski, H. Reimerdes, T.S. Taylor, A.D. Turnbull, M.R. Wade, and S.K. Wong Phys. Plasmas 9, 1997 (2002).

[5] M.S. Chu, J.M. Greene, T.H. Jensen, R.L. Miller, A. Bondeson, R.W. Johnson, and M.E. Mauel, Phys. Plasmas 2, 2236 (1995).